



30 1 Introduction

31 Geochemical data from deep-time marine sediments are fundamental for reconstructing the evolution
32 of the Earth system. By analysing the concentrations of chemical elements in sediments and their
33 isotopic compositions, we can reconstruct the past cycling of elements in the Earth's surface systems
34 and reveal its evolution through time (Large et al., 2015; Reinhard et al., 2017; Farrell et al., 2021;
35 Planavsky et al., 2023). For instance, total organic carbon (TOC), phosphorus (P), biogenic barium
36 (Ba_{bio}), copper (Cu), zinc (Zn), nickel (Ni), etc., enable reconstruct marine primary productivity and
37 carbon cycle changes, thereby revealing past climate change mechanisms (Scott et al., 2013; Schoepfer
38 et al., 2015; Shen et al., 2015; Schoepfer et al., 2016; Xiang et al., 2018; Jin et al., 2020; Tribovillard,
39 2021; Wang et al., 2022; Zhang et al., 2022; Li et al., 2023; Sweere et al., 2023; Zhao et al., 2023).
40 Elements such as uranium (U), vanadium (V), and molybdenum (Mo) can reveal how marine redox
41 conditions changed during critical periods in animal evolution, including mass extinctions and
42 evolutionary radiations (Algeo and Liu, 2020; Schobben et al., 2020; Stockey et al., 2024). Oxygen
43 isotopes ($\delta^{18}O$) in the remains of marine fossil animals can reveal oceanic palaeo-temperature changes
44 (Veizer and Prokoph, 2015; Song et al., 2019; Grossman and Joachimski, 2020; Scotese et al., 2021;
45 Judd et al., 2022). However, many geochemical studies focused on high-resolution research of limited
46 time intervals and/or regions, and there is little comprehensive exploration across large-scale geological
47 time and globally.

48 Fortunately, with more journals and institutions adopting strict data archiving rules and promoting
49 adherence to FAIR (Findability, Accessibility, Interoperability, and Reusability) principles (Wilkinson
50 et al., 2016; "FAIR Play in Geoscience Data," 2019), a large amount of geochemical data has become
51 accessible, and sample meta-data records are more detailed. Several geochemical databases of varying
52 scales and foci have emerged, such as the following:

- 53 ● EarthChem, which covers igneous, sedimentary, and metamorphic rocks and comprises numerous
54 joint databases (<https://www.earthchem.org/>, last accessed: 16 July 2024).
- 55 ● Petrological Database of the Ocean Floor (PetDB), which includes elemental chemical, isotopic,
56 and mineralogical data of global ocean floor igneous rocks, metamorphic rocks, minerals, and
57 inclusions (<https://www.earthchem.org/petdb>, last accessed: 16 July 2024).
- 58 ● Geochemistry of Rocks of the Oceans and Continents (GEOROC), a comprehensive compilation



59 of chemical, isotopic, and other data on igneous rock samples, including whole rock, glass, mineral,
60 and inclusion analyses and metadata (<http://georoc.mpch-mainz.gwdg.de>, last access: 16 July
61 2024).

62 ● Data Publisher for Earth & Environmental Science (PANGAEA), which is used for archiving,
63 publishing, and disseminating georeferenced data from earth, environmental, and biodiversity
64 sciences and includes a large number of sediment core data (<https://www.pangaea.de>, last accessed:
65 16 July 2024).

66 ● Stable Isotope Database for Earth System Research (StabisoDB) containing $\delta^{18}\text{O}$ and $\delta^{13}\text{C}$ data for
67 more than 67,000 macrofossil and microfossil samples, including benthic and planktonic
68 foraminifera, benthic and nektonic mollusks, brachiopods, fish teeth, and conodonts
69 (<https://cnidaria.nat.uni-erlangen.de/stabisodb/>, last accessed: 16 July 2024).

70 ● Sedimentary Geochemistry and Paleoenvironments Project (SGP), which collects multi-proxy
71 sedimentary geochemical data with an emphasis on Neoproterozoic-Palaeozoic shale data in its
72 first data release (<https://sgp-search.io/>, last accessed: 12 June 2024).

73 Many other government initiatives also host databases:

74 ● The United States Geological Survey (USGS) National Geochemical Database, an archive of
75 geochemical information and related metadata from USGS research
76 ([https://www.usgs.gov/energy-and-minerals/mineral-resources-program/science/national-geochemi-
77 cal-database](https://www.usgs.gov/energy-and-minerals/mineral-resources-program/science/national-geochemical-database), last accessed: 16 July 2024).

78 ● The British Geological Survey (BGS), which provides data and information on UK geology,
79 boreholes, geomagnetism, groundwater, rocks, etc. (<http://www.bgs.ac.uk/>, last accessed: 16 July
80 2024).

81 ● The Australian National Whole Rock Geochemistry Database (OZCHEM), including chemical
82 compositions of rock, soil, and sediment samples (<https://ecat.ga.gov.au/geonetwork/srv/>, last
83 accessed: 16 July 2024).

84 Although some of these databases (Table 1) include data on ancient marine sediments, they are
85 often limited to specific countries or regions and have certain shortcomings, such as the lack of age
86 data, the absence of many recent publications, missing information from original individual
87 publications, and relatively coarse age resolutions. Thus, we have established the Deep-Time Marine
88 Sedimentary Element Database (DM-SED), which focuses on the elemental content changes in marine



89 sediments across geological history. The current version of the DM-SED database contains 63,691
 90 entries, enabling research on a series of scientific issues related to palaeoenvironmental, palaeoclimatic,
 91 and elemental cycles in deep-time Earth history.

92 **Table 1. Overview of different databases (Note: not all databases have a clear number of records).**

Database name	Content	Website information	Number of records	Data regions
EarthChem	Igneous, sedimentary, and metamorphic rocks; various joint databases	https://www.earthchem.org/ , last accessed: 16 July 2024	Over 2,596 digital content files in EarthChem Library	Global
PetDB	Elemental chemical, isotopic, and mineralogical data of global ocean floor rocks	https://www.earthchem.org/petdb , last accessed: 16 July 2024	over 6,000,000 samples	Global
GEOROC	Chemical, isotopic, and other data on igneous rock samples	http://georoc.mpch-mainz.gwdg.de , last access: 16 July 2024	672,990 samples	Global
PANGAEA	Georeferenced data from earth, environmental, and biodiversity sciences	https://www.pangaea.de , last accessed: 16 July 2024	Extensive dataset	Global
StabisoDB	$\delta^{18}\text{O}$ and $\delta^{13}\text{C}$ data for macrofossil and microfossil samples	https://cnidaria.nat.uni-erlangen.de/stabisodb/ , last accessed: 16 July 2024	Over 67,000 samples	Global
SGP	Multi-proxy sedimentary geochemical data from the Palaeozoic and Neoproterozoic	https://sgp-search.io/ , last accessed: 12 June 2024	82,578 samples	Global
USGS	Geochemical information and related metadata from USGS research	https://www.usgs.gov/energy-and-minerals/mineral-resources-program/science/national-geochemical-database , last accessed: 16 July 2024	Extensive dataset	United States
BGS	Data on UK geology, boreholes, geomagnetism, groundwater, rocks, etc.	http://www.bgs.ac.uk/ , last accessed: 16 July 2024	Extensive dataset	United Kingdom
OZCHEM	Chemical compositions of rock, soil, and sediment samples	https://ecat.ga.gov.au/geonetwork/srv/ , last accessed: 16 July 2024	Extensive dataset	Australia



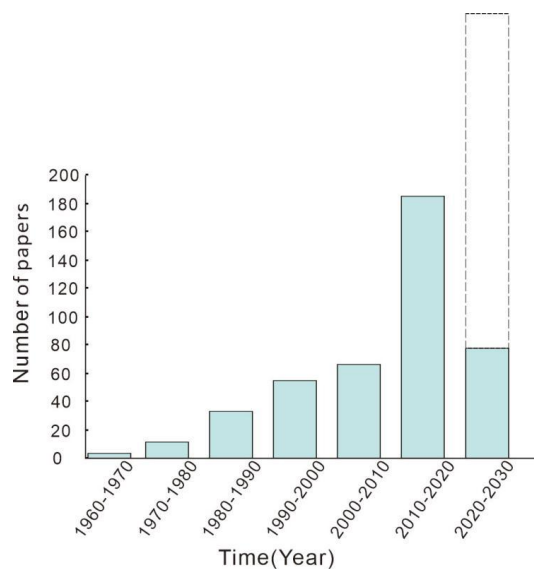
93

94 DM-SED version 0.0.1 is presented in table (.csv) format. Dynamic versions of the most recent
95 release can be found on Zenodo (<https://doi.org/10.5281/zenodo.13898366>, last accessed: 7 October
96 2024) (Lai et al., 2024), and a static copy of Version 0.0.1 is archived in the Geobiology data
97 (<http://202.114.198.132/dmgeo-geobiology-portal/>, last accessed: 25 September 2024). In the following
98 sections, we provide a brief overview of the database, information on the data sources and selection
99 criteria, and a review of the definitions and decisions behind the metadata fields associated with each
100 proxy measurement. We explore the spatial and temporal distribution trends of the compiled data and
101 discuss future uses and limitations of the database.

102

103 **2 Dataset overview**

104 The DM-SED aims at collecting geochemical data from deep-time marine sediments. It is
105 primarily based on the SGP database, but with 34,938 entries of new compiled data. The SGP has a
106 total of 82,578 entries, we selected only 28,753 entries on marine sedimentary geochemical data, and is
107 comprised of three parts: two parts from the U.S. Geological Survey (USGS), i.e. the National
108 Geochemical Database (USGS NGDB, <https://mrdata.usgs.gov/ngdb/rock>, last accessed: 9 September
109 2024) and the Global Geochemical Database for Critical Metals in Black Shales project (USGS
110 CMIBS, Granitto et al., 2017), with samples mainly from North America and Phanerozoic shales from
111 various continents, respectively (Farrell et al., 2021). The third part comprises direct inputs by SGP
112 members. The direct inputs in the Phase 1 SGP data release primarily focused on
113 Neoproterozoic–Palaeozoic shales, although there are other lithologies and other time periods
114 represented (Farrell et al., 2021). Our DM-SED database, built upon the SGP, includes a new
115 compilation of 34,938 entries from 433 literatures, covering a time range from approximately 3800 Ma
116 to the present, and including entries from North America, Europe, Asia, Africa, South America,
117 Oceania, Pacific and Atlantic, thus supplementing the temporal and spatial distribution gaps in the SGP
118 database and thereby creating a more comprehensive sedimentary marine geochemical database. The
119 new compiled literatures span the time range from 1965 to 2023, with the number of papers per decade
120 gradually increasing (Fig. 1). It should be noted that the top of the DM-SED version 0.0.1 data is the
121 new compilation, and the bottom contains data imported from SGP.



122

123 **Figure 1. The distribution of publication years for newly compiled literature (the dashed line denotes the**
 124 **predicted literature from 2023 to 2030).**

125

126 **Table 2. Summary of data entries and points in the DM-SED.**

	Entries	Data points
New compilation	34,938	1,345,589
SGP	28,753	1,066,496
DM-SED	63,691	2,412,085

127

128 The DM-SED database comprises 63,691 entries with 2,412,085 discrete data points (Table 2),
 129 each including location (SampleID, SampleName, SiteName, Region, Elevation, SampleDepth,
 130 ModLat, ModLon, PalaeoLat, PalaeoLon), age (Age, Period, Stage, Biozone), stratigraphic information
 131 (LithName, LithType, Formation, Facies), carbon element (total carbon (Total C), inorganic carbon
 132 (C_{inorg}), TOC, in wt%, isotopic values ($\delta^{18}O_{carb}$, $\delta^{13}C_{Ker}$, $\delta^{13}C_{TOC}$, $\delta^{13}C_{carb}$, $\delta^{34}S_{CAS}$, $\delta^{34}S_{pyr}$, $\delta^{15}N_{total}$,
 133 $\delta^{15}N_{org}$, in ‰), major element (P, Al, Si, Ti, Fe, Ca, Mg, Na, K, S, N, in wt%), trace element (Ag, Ar,
 134 As, B, Ba, Be, Bi, Br, Cd, Ce, Co, Cr, Cs, Cu, Dy, Er, Eu, Ga, Gd, Ge, Hf, Hg, Ho, In, La, Li, Lu, Mn,
 135 Mo, Nb, Nd, Ni, Pb, Pr, Rb, Re, Sb, Sc, Se, Sm, Sn, Sr, Ta, Tb, Te, Th, Tl, Tm, U, V, W, Y, Yb, Zn, Zr,
 136 in ppm), and data sources (Reference, Project). The specific names and descriptions of each field in the
 database are shown in Table 3. The standards and descriptions of isotope ratios in the database are



137 shown in Table 4.

138 **Table 3. Field names and descriptions.**

Field name	Description of field (units)
Location fields	
SampleID	Unique sample identification code
SampleName	Author denoted title for the sample (often non-unique)
SiteName	Name of the drill core site or section
Region	Country or ocean of the data collection site
Elevation	Distance between sampling location and sea level (m)
SampleDepth	Stratigraphic height or depth (m)
ModLat	Modern latitude of collection site rounded to two decimals; negative values indicate the Southern Hemisphere (decimal degrees)
ModLon	Modern longitude of the collection site rounded to two decimals; negative values indicate the Western Hemisphere (decimal degrees)
PalaeoLat	Palaeolatitude of collection site rounded to two decimals; negative values indicate the Southern Hemisphere (decimal degrees)
PalaeoLon	Palaeolongitude of the collection site rounded to two decimals; negative values indicate the Western Hemisphere (decimal degrees)
Age fields	
Age	Absolute Age, in reference to GTS2020 (Ma)
Period	The geologic period
Stage	The geologic stage (i.e. geochronologic age)
Biozone	Conodont, graptolite, ammonite biozone, etc
Stratigraphy	
LithName	Lithological name of the sample, as originally published
LithType	Lithology type of sample (e.g. carbonate, siliciclastic)
Formation	Geologic formation name
Facies	Depositional environment (e.g. mid-shelf, ramp)
Proxy fields	
Carbon	The content of carbon, including Total C, C _{inorg} , TOC, rounded to two decimals (wt%)
Isotopes	The isotope value, rounded to two decimals (‰)
Major elements	The content of major elements such as P, Al, and Si, rounded to two decimals (wt%)
Trace elements	The content of trace elements such as Ag, Ar, As, B, and Ba, rounded to two decimals (ppm)
Data sources	
Reference	Data sources, including published literature or other databases
Project	Two parts: new compilation and SGP

139

140

141



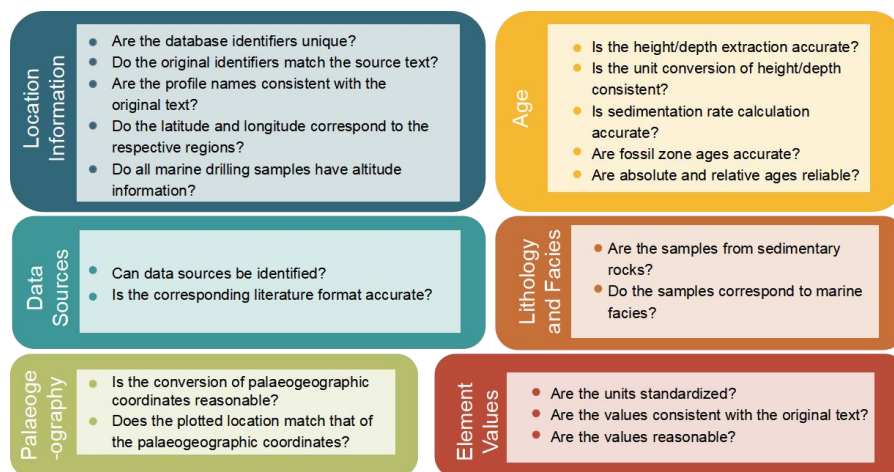
142 **Table 4. Standards and descriptions of isotope ratios in the DM-SED.**

Symbol	Standard	Description
$\delta^{18}\text{O}_{\text{carb}}$	Vienna Pee Dee Belemnite (VPDB)	Oxygen isotope ratio of carbonate minerals, used in palaeoclimate studies.
$\delta^{13}\text{C}_{\text{ker}}$	VPDB	Carbon isotope ratio of kerogen, used to study the source and depositional environment of organic matter.
$\delta^{13}\text{C}_{\text{TOC}}$	VPDB	Carbon isotope ratio of total organic carbon, used to analyse the source of organic matter and biogeochemical cycles in sediments.
$\delta^{13}\text{C}_{\text{carb}}$	VPDB	Carbon isotope ratio of carbonate minerals, used in palaeoclimate and carbon cycle research.
$\delta^{34}\text{S}_{\text{CAS}}$	Vienna Canyon Diablo Troilite (VCDT)	Sulfur isotope ratio of carbonate-associated sulfate, used to study the sulfur cycle and redox conditions.
$\delta^{34}\text{S}_{\text{pyr}}$	VCDT	Sulfur isotope ratio of pyrite, typically used to investigate the sulfur cycle and redox conditions in ancient oceans.
$\delta^{15}\text{N}_{\text{total}}$	Atmospheric Nitrogen (air N_2)	Nitrogen isotope ratio of total nitrogen, used to study the nitrogen cycle and nutrient sources.
$\delta^{15}\text{N}_{\text{org}}$	air N_2	Nitrogen isotope ratio of organic nitrogen, often used to analyse the source of organic matter and the nitrogen cycle.

143

144 **3 Dataset screening and processing**

145 This section details the screening and processing criteria for sample location, age, lithology and facies,
 146 specific geochemical values, and data source information (Fig. 2).



147

148 **Figure 2. The data filtering and processing criteria for DM-SED.**

149 For sample location, the dataset includes SampleID, SampleName, SiteName, Region, Elevation,
150 SampleDepth, ModLat, ModLon, PalaeoLat, and PalaeoLon. A unique SampleID is assigned to each
151 sample in the DM-SED. The SampleName corresponds to the identifier given in each referenced
152 publication, facilitating cross-referencing with the original data. The SiteName includes well name or
153 outcrop information, representing the smallest unit of location information. The Region indicates the
154 country or ocean area where the sample has been collected and represents a broader geographical range.
155 The Elevation data are mainly related to samples from the Deep Sea Drilling Project (DSDP) and the
156 Ocean Drilling Program (ODP) collected from post-Cretaceous sediments and indicate whether the
157 samples originate from deep or shallow marine environments. SampleDepth refers to the relative
158 position (in metres) of the sample within the well or outcrop, which is crucial for calculating sample
159 age. In some publications, specific heights are not provided directly but are given as relative heights
160 through figures. We manually extracted these heights using WebPlotDigitizer, rounding to two decimal
161 places (Drevon et al., 2017). For publications in which heights are expressed in feet or centimetres, we
162 converted the units to metres. Modern latitude and longitude (ModLat and ModLon) information are
163 the most precise location data. Although some publications provide exact coordinates, many offer only
164 section names (i.e. SiteName) and regions or merely a map marking the location of the section. For
165 publications providing section names, we determined accurate coordinates by consulting other studies
166 carried out in the same section. For those providing only a map marking the location of the section, we
167 used Google Maps to estimate relative coordinates. To ensure consistency, we recorded sample



168 coordinates in decimal degrees, rounded to two decimal places, with positive values indicating north
169 latitude and east longitude and negative values indicating south latitude and west longitude. For
170 palaeo-coordinates, we reconstructed palaeo-latitude and palaeo-longitude (PalaeoLat, and PalaeoLon)
171 using the sample age and modern coordinates, employing the PointTracker v7 rotation files from the
172 PALEOMAP project, which are based on current geographic reference data and global tectonic history
173 models (Scotese, 2008). It is important to note that we only generated palaeogeographic locations for
174 samples from the Phanerozoic, as the geological records from this time are more complete and
175 abundant compared to those from the Precambrian, making the reconstruction of geographic features
176 (such as ancient oceans, mountains, plains, etc.) relatively more reliable and accurate (Scotese and
177 Wright 2018). We plotted the sample points on palaeogeographic maps based on Scotese's data using
178 QGIS 3.16 (Scotese and Wright 2018).

179 To assign specific ages to each sample in the database, we assumed a constant sedimentation rate
180 within the same formation or group of section. If the original studies provided numerical ages for two
181 or more samples, we calculated the precise age for each sample based on the sedimentation rate and
182 assigned it accordingly. If absolute ages were not provided in the original literature, we assigned
183 approximate ages based on corresponding fossil zones or the general age of the same lithostratigraphic
184 unit in the same region (Farrell et al., 2021; Judd et al., 2022). For samples with completely missing
185 height information in the original text, we assigned the same age to all samples within the section based
186 on lithostratigraphic information (mainly samples from USGS NGDB and USGS CMIBS). Once each
187 sample had a specific age, we assigned it to a specific Period and Stage according to its age. We
188 attempted to incorporate the most recent age models; however, due to the extensive size of the data
189 compilation, it was not feasible to update all of them. All ages were based on the timescale provided by
190 the Geologic Time Scale 2020 (Gradstein et al., 2020).

191 For lithology and facies, the lithologies include shale, mudstone, sandstone, limestone, dolomite,
192 and others. We classified these into two major types of rock: siliciclastic sedimentary rocks (88.7%)
193 and carbonate rocks (11.3%). For outcrop sections, lithostratigraphic unit was generally available;
194 however, for marine drilling data, there were no corresponding group names. Regarding facies
195 classification, before the Cretaceous, the primary depositional environment was marine settings on
196 continental crust, including specific facies such as tidal flats, inner shelves, outer shelves, and basinal.
197 However, after the Cretaceous, with most samples coming from DSDP and ODP, deep ocean



198 depositional environments emerged.

199 For specific geochemical values in the DM-SED database, we standardized the units, converting
200 oxides to elements (e.g. P (ppm) to P (wt%), P₂O₅ (wt%) to P (wt%)). If a sample was analysed
201 multiple times, we averaged the value. For literature before 2000, some data were preserved as images,
202 requiring manual extraction of values, and some images were slightly blurry, potentially leading to
203 minor human error. We excluded data that were beyond detection limits (e.g. the trace element content
204 is too low and the value provided in the text represents the minimum detection limit) or unreasonable
205 (e.g. negative values for major and trace elements).

206 Regarding data sources, we ensured that each corresponding reference was collected and listed in
207 full citation format, including authors, title, publication date, journal, page numbers, and DOI. Most
208 data in the SGP database came directly from USGS NGDB and USGS CMIBS, without corresponding
209 literature sources, so we marked them individually. And the project includes two parts: new
210 compilation and SGP. We used keyword searches in Google Scholar to identify missing references and
211 made efforts to target literature for data-scarce regions (e.g. South America) and time intervals (e.g.
212 Silurian, Jurassic).

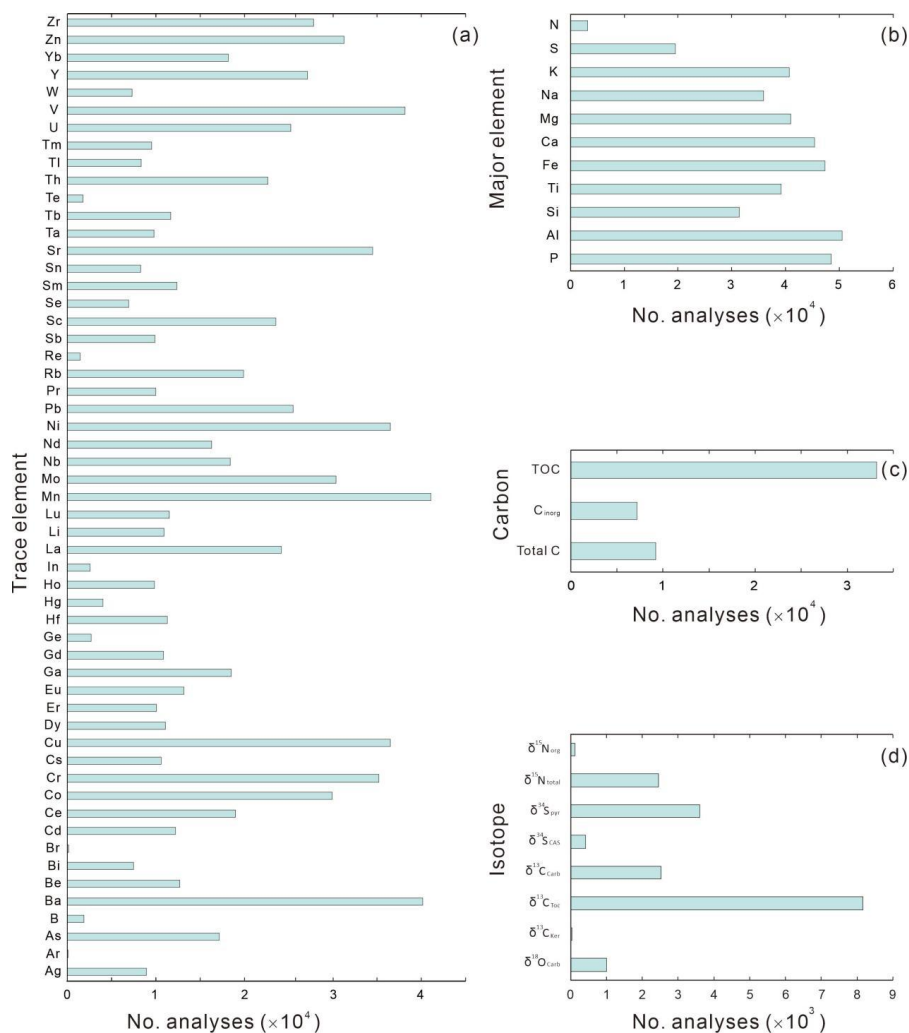
213 **4 Data distribution**

214 The elemental data content distribution for the entire database is shown in Fig. 3. Overall, major
215 elements have the highest data quantity, followed by trace elements and carbon elements, with isotope
216 data having the lowest quantity. Among the major elements, N has the fewest entries, with 3,164
217 records, whereas the other major elements all have more than 10,000 entries. Al has the highest
218 quantity, with 50,568 records. Among trace elements, Mn has the largest record (41,058 records),
219 followed by Ba (40,163 records). Ar and Br have the fewest records, with 9 and 162 records,
220 respectively. Other elements such as Ag, B, Bi, Ge, Hg, Ho, In, Pr, Re, Sb, Se, Sn, Ta, Te, Tl, Tm, and
221 W have data quantities ranging from 1,000 to 10,000. Elements such as As, Be, Cd, Ce, Co, Cr, Cs, Cu,
222 Dy, Er, Eu, Ga, Gd, Hf, La, Li, Lu, Mo, Nb, Nd, Ni, Pb, Rb, Sc, Sm, Sr, Tb, Th, U, V, Y, Yb, Zn, and
223 Zr all have more than 10,000 records each. For carbon elements, TOC has the most records, with
224 33,216 entries, followed by Total C with 9,201 entries. C_{inorg} has the fewest records, with 7,194 entries.
225 Isotope data are overall less abundant, with none exceeding 10,000 entries; the most abundant is



226 $\delta^{13}\text{C}_{\text{TOC}}$, with 8,166 records, and the least abundant is $\delta^{13}\text{C}_{\text{Ker}}$, with only 29 records.

227



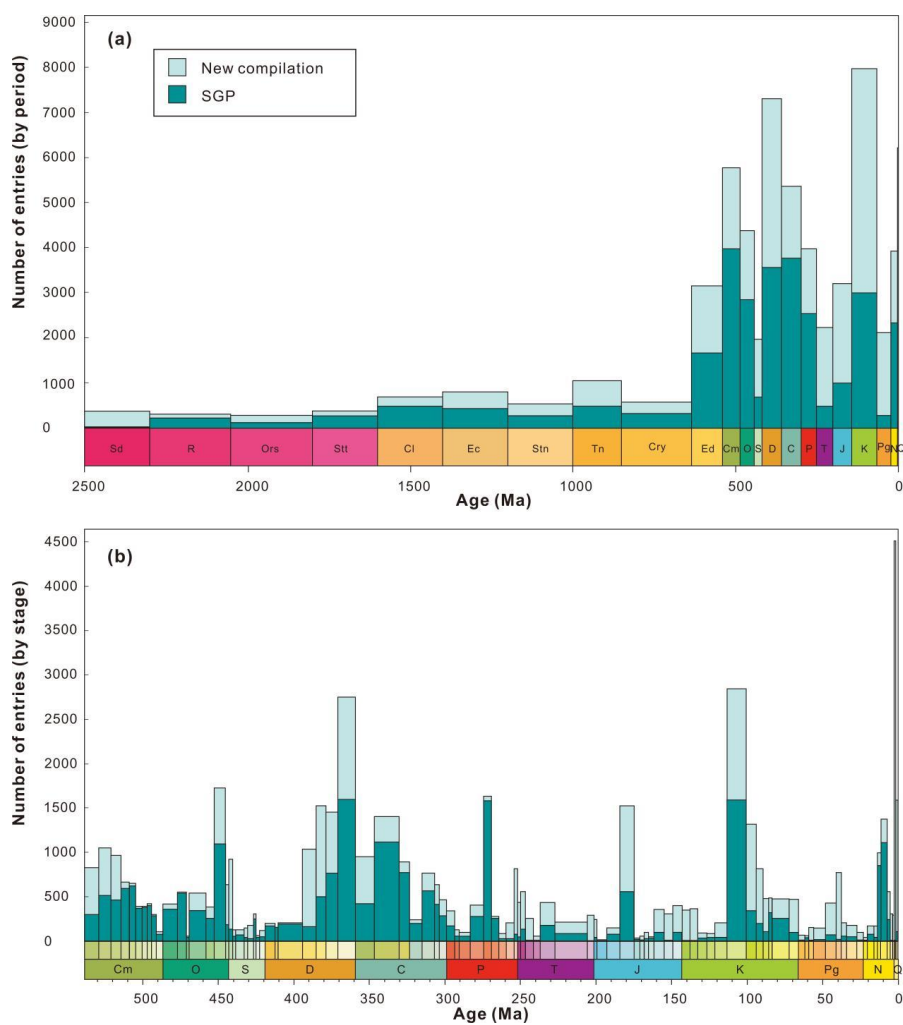
228

229 **Figure 3. Histogram distribution of different subsets. (a) Trace elements. (b) Major elements. (c) Carbon**
 230 **elements. (d) Isotopes.**

231 The temporal trend of data density in the entire database, shown in Fig. 4a, indicates that the data
 232 are primarily distributed in the Phanerozoic Eon, which accounts for 85% of the entire database. From
 233 this, the Cenozoic Era accounts for 19% of the database, the Mesozoic Era accounts for 21%, and the
 234 Palaeozoic Era accounts for 45%. Precambrian data account for only 15% of the entire database. The
 235 SGP data are most concentrated in the Palaeozoic Era, in which they make up 27% of the total database,



236 with the new compiled data contributing only 18%. In other eras, the new compiled data outnumber the
 237 SGP data: 4% versus 15% in the Cenozoic, 7% versus 14% in the Mesozoic, and 7% versus 8% in the
 238 Precambrian. This is mainly the case because the SGP data in the first phase were primarily from the
 239 Neoproterozoic and Palaeozoic eras (Farrell et al., 2021).
 240

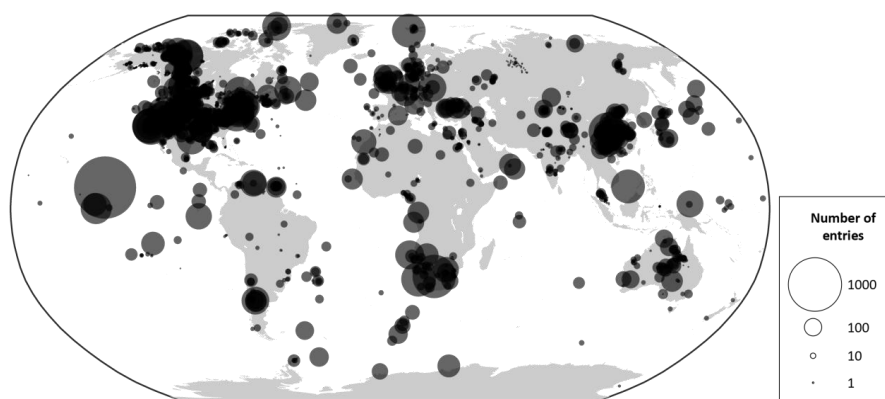


241
 242 **Figure 4. The age distribution of samples in the database. (a) Age distribution of samples (excluding a small**
 243 **number of samples with ages >2500 Ma from the figure, a total of 1298 samples). (b) Age distribution of**
 244 **Phanerozoic samples at the stage level.**

245
 246



247 For the distribution of sample ages within the Phanerozoic, we divided the samples by stage, as
248 shown in Fig. 4b. For the Quaternary Period, due to its short duration, data were not subdivided by
249 Stage, but only into Holocene and Pleistocene. Data distribution is not uniform, with the highest
250 concentration in the Quaternary Period. These data mainly come from DSDP and ODP, which are
251 characterised by a high number of core samples and high resolution. There are fewer data for the Upper
252 Permian, Lower Triassic, and Lower to Middle Jurassic, possibly because of the existence of Pangaea
253 at that time, which reduced the area of continental margins and inhibited marine transgressions,
254 resulting in fewer preserved marine environments in comparison to those of other geological periods
255 (Mackenzie and Pigott, 1981; Walker et al., 2002). The distribution of sample quantities in other
256 periods fluctuates, often corresponding to periods of significant research interest, such as the
257 end-Ordovician, end-Devonian, end-Permian, Early Jurassic Toarcian and Early Cretaceous Albian,
258 which had peaks in sample numbers due to their association with major mass extinction events and
259 oceanic anoxic events (Fan et al., 2020).



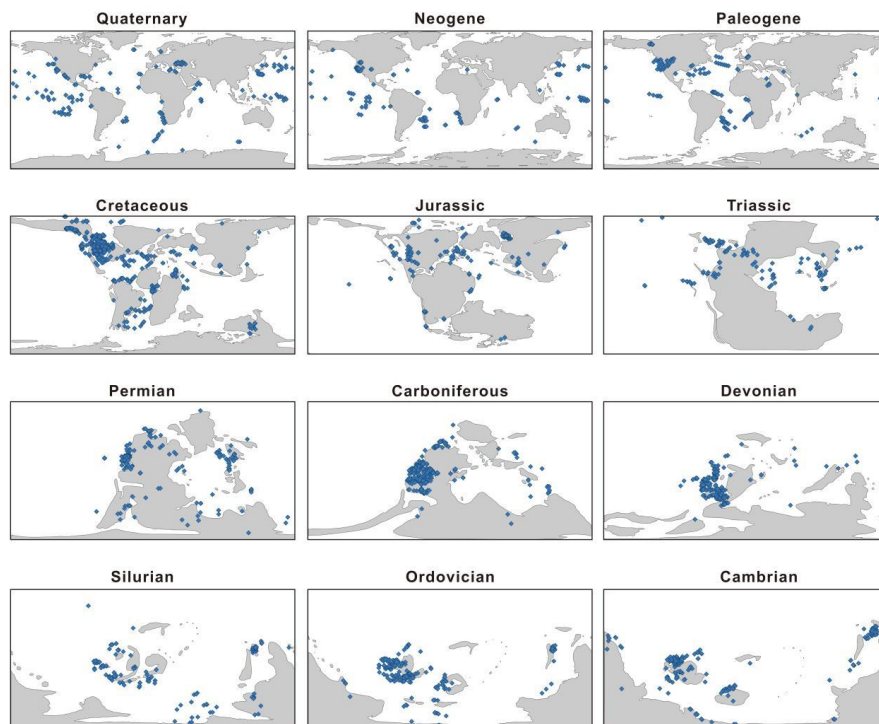
260

261 **Figure 5. Bubble chart of modern geographical distribution and sample quantities in the database.**

262 In terms of spatial trends, the spatial distribution of sampling points in the DM-SED database is
263 inherently uneven, both in modern and palaeogeographic locations. Modern locations are primarily
264 concentrated in North America, Europe, South Africa, and China (Fig. 5). When modern coordinates
265 are converted to palaeogeographic coordinates and projected onto palaeogeographic maps, Cambrian to
266 Jurassic data come predominantly from continental margin environments, as oceanic crust plates
267 subducting before the Cretaceous led to preservation of very few deep-sea environments (Fig. 6).
268 Cambrian and Ordovician data are distributed mainly on the Laurentia, Baltica, and South China plates,



269 with a few along the Gondwana margin. Silurian data occur mainly on Laurentia, South China, and
270 right side of Gondwana. Devonian and Carboniferous data are primarily on the Laurussia plate, with
271 sparse distribution in South China and Gondwana. Permian and Triassic data are mainly on the
272 Laurussia and South China plates, with sparse distribution in Gondwana. Jurassic data are primarily on
273 the North American, European shelf, with sparse distribution on other plates. From the Cretaceous to
274 the Quaternary, sample locations, dominated by data from the DSDP, ODP, and USGS NGDB projects,
275 are mainly in the deep oceans and North America.

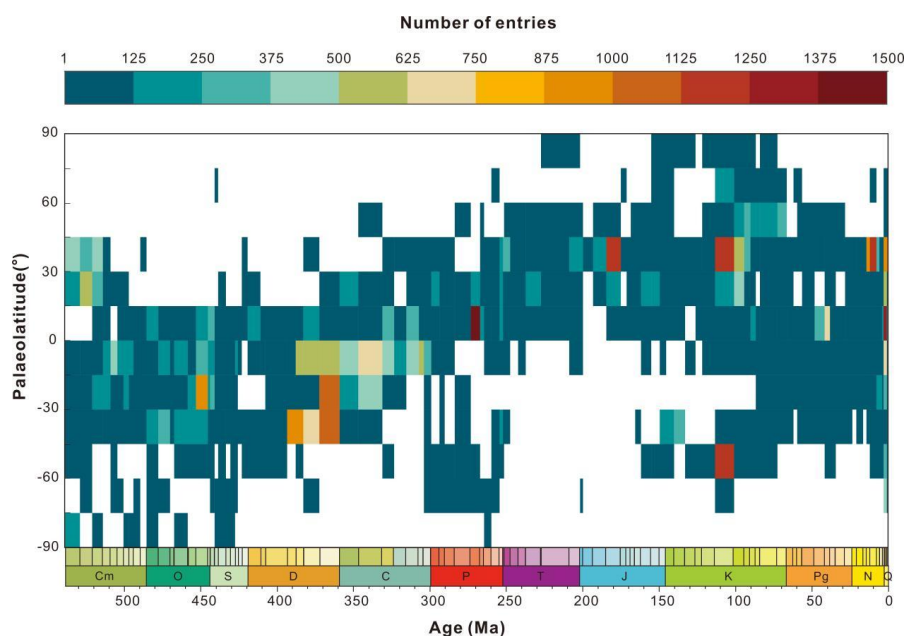


276
277 **Figure 6. The palaeogeographic distribution of sample sites in the DM-SED.**

278 When averaging all Phanerozoic data by stage and spatially averaging them into 15°
279 palaeolatitudes bins (Fig. 7), Palaeozoic data records are mainly biased toward tropical regions.
280 Cambrian data are concentrated between 15° S and 30° N, Ordovician to Carboniferous data are
281 concentrated between 45° S and 15° N, and Permian data are concentrated between 0° N and 30° N,
282 with data mainly fluctuating around the equator. As continents migrated northward through the
283 Mesozoic and into the Cenozoic, records began to show bias toward mid-latitudes in the Northern
284 Hemisphere. From the Triassic to the Cretaceous, data are mainly concentrated between 0° N and 60°



285 N.



286

287 **Figure 7. The spatiotemporal distributions of sample quantities (categorized temporally by stage and**
288 **spatially by palaeolatitude intervals of 15°).**

289

290 5 Usage instructions

291 The ultimate goal of the DM-SED database is to provide the geoscience community with a valuable
292 resource of knowledge and geographic information. By deriving meaningful conclusions from a large
293 marine sediment geochemistry dataset, we aim to enhance our understanding of Earth's environmental
294 changes over time and space. All entries in DM-SED contain the source of original proxy values,
295 ensuring traceability between DM-SED and the original datasets from which the data were extracted.

296 However, our database has some limitations. The criteria for age determination, relying variously
297 on fossil zones and lithostratigraphic unit information, are not entirely uniform. Some age
298 determinations are still coarse, with samples from a single section were assigned the same age.
299 Additionally, the data quantity for some elements is still low. The testing methods for elements are not
300 annotated, and there may be significant differences in methodological precision between older and
301 newer literature. Currently, these issues remain largely unresolved. Despite our best efforts to identify



302 data from the literature and process quality control for each entry, the sheer volume of data in DM-SED
303 means that some errors or omissions are inevitable. Prompt corrections and continuous updates are
304 expected to ensure the credibility of this dataset.

305 Finally, it is important to recognize that DM-SED merely compiles these various datasets and
306 cannot impose any requirements on their generation. When using the data (and where practicable), we
307 recommend citing both DM-SED and the original data sources to ensure proper attribution.

308

309 **6 Data availability**

310 Version controlled releases of the DM-SED can be found on Zenodo
311 (<https://doi.org/10.5281/zenodo.13898366>, last accessed: 7 October 2024) (Lai et al., 2024). A static
312 copy of DM-SED version 0.0.1 is archived in the Geobiology data
313 (<http://202.114.198.132/dmgeo-geobiology-portal/>, last accessed: 25 September 2024). We plan to
314 supplement and improve the dataset continuously and hope to collaborate with existing compilation
315 authors to assist in adding new content.

316

317 **7 Code availability**

318 The software tools used in this study are available at the following links: WebPlotDigitizer can be
319 downloaded from <https://github.com/automeris-io/WebPlotDigitizer/releases> (last accessed: 20 July
320 2024); the PointTracker v7 tool can be found at <http://www.paleogis.com> (last accessed: 20 July 2024);
321 QGIS 3.16 can be downloaded from the <https://qgis.org/project/overview/> (last accessed: 20 July
322 2024).

323

324 **Author contributions.** Jiankang Lai: Writing – original draft, Visualization, Data collection,
325 Investigation. Haijun Song: Writing – review & editing, Supervision, Investigation, Funding
326 acquisition. Daoliang Chu: Writing – review & editing, Investigation. Jacopo Dal Corso: Writing –
327 review & editing, Investigation. Erik A. Sperling: Writing – review & editing, Investigation.

328 Yuyang Wu: Writing – review & editing, Supervision, Investigation, Data collection. Xiaokang Liu:



329 Writing– review & editing, Investigation. Lai Wei: Writing– review & editing, Data collection,
330 Investigation. Mingtao Li: Writing– review & editing, Investigation. Hanchen Song: Writing– review
331 & editing, Investigation. Yong Du: Writing– review & editing, Investigation. Enhao Jia: Writing–
332 review & editing, Investigation. Yan Feng: Writing– review & editing, Investigation. Huyue Song:
333 Writing– review & editing, Investigation. Wenchao Yu: Writing– review & editing, Investigation.
334 Qingzhong Liang: Writing– review & editing, Investigation. Xinchuan Li: Writing– review & editing,
335 Investigation. Hong Yao: Writing– review & editing, Investigation.

336

337 **Competing interests.** The authors declare that they have no conflicts of interest.

338

339 **Acknowledgements.**

340 We thank Xiang Shu for the discussions on analytical methods. This paper benefited greatly from
341 comments from xxx anonymous reviewers.

342

343 **Funding:**

344 This study was supported by the National Natural Science Foundation of China grant 42325202, the
345 State Key R&D Project of China (2023YFF0804000), 111 Project grant B08030, and Natural Science
346 Foundation of Hubei (2023AFA006). E.A.S. is supported by United States National Science
347 Foundation grant EAR-2143164.

348

349 **REFERENCES**

350 Algeo, T. J. and Liu, J.: A re-assessment of elemental proxies for paleoredox analysis, *Chem. Geol.*,
351 540, 119549, <https://doi.org/10.1016/j.chemgeo.2020.119549>, 2020.

352 Drevon, D., Fursa, S. R., and Malcolm, A. L.: Intercoder Reliability and Validity of WebPlotDigitizer
353 in Extracting Graphed Data, *Behav. Modif.*, 41, 323-339,
354 <https://doi.org/10.1177/0145445516673998>, 2017.

355 FAIR .: FAIR Play in geoscience data, *Nat. Geosci.*, 12, 961,
356 <https://doi.org/10.1038/s41561-019-0506-4>, 2019.



- 357 Fan, J., Shen, S., Erwin, D. H., Sadler, P. M., MacLeod, N., Cheng, Q., Hou, X., Yang, J., Wang, X.,
358 Wang, Y., Zhang, H., Chen, X., Li, G., Zhang, Y., Shi, Y., Yuan, D., Chen, Q., Zhang, L., Li, C.,
359 and Zhao, Y.: A high-resolution summary of Cambrian to Early Triassic marine invertebrate
360 biodiversity, *Science*, 367, 272-277, <https://doi.org/10.1126/science.aax4953>, 2020.
- 361 Farrell, U. C., Samawi, R., Anjanappa, S., Klykov, R., Adeboye, O. O., Agic, H., Ahm, A. C., Boag, T.
362 H., Bowyer, F., Brocks, J. J., Brunoir, T. N., Canfield, D. E., Chen, X., Cheng, M., Clarkson, M.
363 O., Cole, D. B., Cordie, D. R., Crockford, P. W., Cui, H., Dahl, T. W., Mouro, L. D., Dewing, K.,
364 Dornbos, S. Q., Drabon, N., Dumoulin, J. A., Emmings, J. F., Endriga, C. R., Fraser, T. A.,
365 Gaines, R. R., Gaschnig, R. M., Gibson, T. M., Gilleaudeau, G. J., Gill, B. C., Goldberg, K.,
366 Guilbaud, R., Halverson, G. P., Hammarlund, E. U., Hantsoo, K. G., Henderson, M. A.,
367 Hodgskiss, M. S. W., Horner, T. J., Husson, J. M., Johnson, B., Kabanov, P., Brenhin Keller, C.,
368 Kimmig, J., Kipp, M. A., Knoll, A. H., Kreitsmann, T., Kunzmann, M., Kurzweil, F., LeRoy, M.
369 A., Li, C., Lipp, A. G., Loydell, D. K., Lu, X., Macdonald, F. A., Magnall, J. M., Mand, K.,
370 Mehra, A., Melchin, M. J., Miller, A. J., Mills, N. T., Mwinde, C. N., O'Connell, B., Och, L. M.,
371 Ossa Ossa, F., Pages, A., Paiste, K., Partin, C. A., Peters, S. E., Petrov, P., Playter, T. L.,
372 Plaza-Torres, S., Porter, S. M., Poulton, S. W., Pruss, S. B., Richoz, S., Ritzer, S. R., Rooney, A.
373 D., Sahoo, S. K., Schoepfer, S. D., Sclafani, J. A., Shen, Y., Shorttle, O., Slotznick, S. P., Smith,
374 E. F., Spinks, S., Stockey, R. G., Strauss, J. V., Stueken, E. E., Tecklenburg, S., Thomson, D.,
375 Tosca, N. J., Uhlein, G. J., Vizcaino, M. N., Wang, H., White, T., Wilby, P. R., Woltz, C. R.,
376 Wood, R. A., Xiang, L., Yurchenko, I. A., Zhang, T., Planavsky, N. J., Lau, K. V., Johnston, D. T.,
377 and Sperling, E. A.: The Sedimentary Geochemistry and Paleoenvironments Project, *Geobiology*,
378 19, 545-556, <https://doi.org/10.1111/gbi.12462>, 2021.
- 379 Gradstein, F. M., Ogg, J. G., Schmitz, M. D., and Ogg, G. M.: *Geologic time scale 2020*, Elsevier,
380 2020.
- 381 Granitto, M., Giles, S. A., and Kelley, K. D.: *Global Geochemical Database for Critical Metals in*
382 *Black Shales*, U.S. Geological Survey data release [data set], <https://doi.org/10.5066/F71G0K7X>,
383 2017.
- 384 Grossman, E. L. and Joachimski, M. M.: *Oxygen Isotope Stratigraphy*, in: *Geologic Time Scale 2020*,
385 279-307, <https://doi.org/10.1016/b978-0-12-824360-2.00010-3>, 2020.
- 386 Jin, C., Li, C., Algeo, T. J., Wu, S., Cheng, M., Zhang, Z., and Shi, W.: Controls on organic matter



- 387 accumulation on the early-Cambrian western Yangtze Platform, South China, *Mar. Pet. Geol.*,
388 111, 75-87, <https://doi.org/10.1016/j.marpetgeo.2019.08.005>, 2020.
- 389 Judd, E. J., Tierney, J. E., Huber, B. T., Wing, S. L., Lunt, D. J., Ford, H. L., Inglis, G. N., McClymont,
390 E. L., O'Brien, C. L., Rattanasriampaipong, R., Si, W., Staitis, M. L., Thirumalai, K., Anagnostou,
391 E., Cramwinckel, M. J., Dawson, R. R., Evans, D., Gray, W. R., Grossman, E. L., Henehan, M. J.,
392 Hupp, B. N., MacLeod, K. G., O'Connor, L. K., Sanchez Montes, M. L., Song, H., and Zhang, Y.
393 G.: The PhanSST global database of Phanerozoic sea surface temperature proxy data, *Sci. Data*, 9,
394 753, <https://doi.org/10.1038/s41597-022-01826-0>, 2022.
- 395 Lai, J., Song, H., Chu, D., Dal Corso, J., Sperling, E. A., Wu, Y., Liu, X., Wei, L., Li, M., Song, H., Du,
396 Y., Jia, E., Feng, Y., Song, H., Yu, W., Liang, Q., Li, X., and Yao, H.: Deep-Time Marine
397 Sedimentary Element Database [data set], Zenodo. <https://doi.org/10.5281/zenodo.13898366>,
398 2024.
- 399 Large, R. R., Halpin, J. A., Lounejeva, E., Danyushevsky, L. V., Maslennikov, V. V., Gregory, D.,
400 Sack, P. J., Haines, P. W., Long, J. A., Makoundi, C., and Stepanov, A. S.: Cycles of nutrient
401 trace elements in the Phanerozoic ocean, *Gondwana Res.*, 28, 1282-1293,
402 <https://doi.org/10.1016/j.gr.2015.06.004>, 2015.
- 403 Li, Z., Zhang, Y. G., Torres, M., and Mills, B. J. W.: Neogene burial of organic carbon in the global
404 ocean, *Nature*, 613, 90-95, <https://doi.org/10.1038/s41586-022-05413-6>, 2023.
- 405 Mackenzie, F. T. and Pigott, J. D.: Tectonic controls of Phanerozoic sedimentary rock cycling, *J. Geol.*
406 *Soc.*, 138, 183-196, <https://doi.org/10.1144/gsjgs.138.2.0183>, 1981.
- 407 Planavsky, N. J., Asael, D., Rooney, A. D., Robbins, L. J., Gill, B. C., Dehler, C. M., Cole, D. B.,
408 Porter, S. M., Love, G. D., Konhauser, K. O., and Reinhard, C. T.: A sedimentary record of the
409 evolution of the global marine phosphorus cycle, *Geobiology*, 21, 168-174,
410 <https://doi.org/10.1111/gbi.12536>, 2023.
- 411 Reinhard, C. T., Planavsky, N. J., Gill, B. C., Ozaki, K., Robbins, L. J., Lyons, T. W., Fischer, W. W.,
412 Wang, C., Cole, D. B., and Konhauser, K. O.: Evolution of the global phosphorus cycle, *Nature*,
413 541, 386-389, <https://doi.org/10.1038/nature20772>, 2017.
- 414 Schobben, M., Foster, W. J., Sleveland, A. R. N., Zuchuat, V., Svensen, H. H., Planke, S., Bond, D. P.
415 G., Marcelis, F., Newton, R. J., Wignall, P. B., and Poulton, S. W.: A nutrient control on marine
416 anoxia during the end-Permian mass extinction, *Nat. Geosci.*, 13, 640-646,



- 417 <https://doi.org/10.1038/s41561-020-0622-1>, 2020.
- 418 Schoepfer, S. D., Algeo, T. J., Ward, P. D., Williford, K. H., and Haggart, J. W.: Testing the limits in a
419 greenhouse ocean: Did low nitrogen availability limit marine productivity during the end-Triassic
420 mass extinction?, *Earth Planet. Sci. Lett.*, 451, 138-148, <https://doi.org/10.1016/j.epsl.2016.06.050>,
421 2016.
- 422 Schoepfer, S. D., Shen, J., Wei, H., Tyson, R. V., Ingall, E., and Algeo, T. J.: Total organic carbon,
423 organic phosphorus, and biogenic barium fluxes as proxies for paleomarine productivity, *Earth*
424 *Sci. Rev.*, 149, 23-52, <https://doi.org/10.1016/j.earscirev.2014.08.017>, 2015.
- 425 Scotese, C.: The PALEOMAP Project PaleoAtlas for ArcGIS, version 1, 2, 16-31, 2008.
- 426 Scotese, C. R., Song, H., Mills, B. J. W., and van der Meer, D. G.: Phanerozoic paleotemperatures: The
427 earth's changing climate during the last 540 million years, *Earth Sci. Rev.*, 215, 103503,
428 <https://doi.org/10.1016/j.earscirev.2021.103503>, 2021.
- 429 Scotese, C. R. and Wright, N.: PALEOMAP Paleodigital Elevation Models (PaleoDEMS) for the
430 Phanerozoic PALEOMAP Project, Paleomap Proj,
431 <https://www.earthbyte.org/paleodem-resourcescotese-and-wright-2018/>, 2018.
- 432 Scott, C., Planavsky, N. J., Dupont, C. L., Kendall, B., Gill, B. C., Robbins, L. J., Husband, K. F.,
433 Arnold, G. L., Wing, B. A., Poulton, S. W., Bekker, A., Anbar, A. D., Konhauser, K. O., and
434 Lyons, T. W.: Bioavailability of zinc in marine systems through time, *Nat. Geosci.*, 6, 125-128,
435 <https://doi.org/10.1038/ngeo1679>, 2012.
- 436 Shen, J., Schoepfer, S. D., Feng, Q., Zhou, L., Yu, J., Song, H., Wei, H., and Algeo, T. J.: Marine
437 productivity changes during the end-Permian crisis and Early Triassic recovery, *Earth Sci. Rev.*,
438 149, 136-162, <https://doi.org/10.1016/j.earscirev.2014.11.002>, 2015.
- 439 Song, H., Wignall, P. B., Song, H., Dai, X., and Chu, D.: Seawater Temperature and Dissolved Oxygen
440 over the Past 500 Million Years, *J. Earth Sci.*, 30, 236-243,
441 <https://doi.org/10.1007/s12583-018-1002-2>, 2019.
- 442 Stockey, R. G., Cole, D. B., Farrell, U. C., Agić, H., Boag, T. H., Brocks, J. J., Canfield, D. E., Cheng,
443 M., Crockford, P. W., Cui, H., Dahl, T. W., Del Mouro, L., Dewing, K., Dornbos, S. Q., Emmings,
444 J. F., Gaines, R. R., Gibson, T. M., Gill, B. C., Gilleaudeau, G. J., Goldberg, K., Guilbaud, R.,
445 Halverson, G., Hammarlund, E. U., Hantsoo, K., Henderson, M. A., Henderson, C. M., Hodgskiss,
446 M. S. W., Jarrett, A. J. M., Johnston, D. T., Kabanov, P., Kimmig, J., Knoll, A. H., Kunzmann, M.,



- 447 LeRoy, M. A., Li, C., Loydell, D. K., Macdonald, F. A., Magnall, J. M., Mills, N. T., Och, L. M.,
448 O'Connell, B., Pagès, A., Peters, S. E., Porter, S. M., Poulton, S. W., Ritzer, S. R., Rooney, A. D.,
449 Schoepfer, S., Smith, E. F., Strauss, J. V., Uhlein, G. J., White, T., Wood, R. A., Woltz, C. R.,
450 Yurchenko, I., Planavsky, N. J., and Sperling, E. A.: Sustained increases in atmospheric oxygen
451 and marine productivity in the Neoproterozoic and Palaeozoic eras, *Nat. Geosci.*, 17, 667-674,
452 <https://doi.org/10.1038/s41561-024-01479-1>, 2024.
- 453 Sweere, T. C., Dickson, A. J., and Vance, D.: Nickel and zinc micronutrient availability in Phanerozoic
454 oceans, *Geobiology*, 21, 310-322, <https://doi.org/10.1111/gbi.12541>, 2023.
- 455 Tribovillard, N.: Re-assessing copper and nickel enrichments as paleo-productivity proxies, *BSGF -*
456 *Earth Sciences Bulletin*, 192, 54, <https://doi.org/10.1051/bsgf/2021047>, 2021.
- 457 Veizer, J. and Prokoph, A.: Temperatures and oxygen isotopic composition of Phanerozoic oceans,
458 *Earth Sci. Rev.*, 146, 92-104, <https://doi.org/10.1016/j.earscirev.2015.03.008>, 2015.
- 459 Walker, L. J., Wilkinson, B. H., and Ivany, L. C.: Continental drift and Phanerozoic carbonate
460 accumulation in shallow-shelf and deep-marine settings, *J. Geol.*, 110, 75-87,
461 <https://doi.org/10.1086/324318>, 2002.
- 462 Wang, D., Liu, Y., Zhang, J., Lang, Y., Li, Z., Tong, Z., Xu, L., Su, Z., and Niu, J.: Controls on marine
463 primary productivity variation and organic matter accumulation during the Late Ordovician –
464 Early Silurian transition, *Mar. Pet. Geol.*, 142, 105742,
465 <https://doi.org/10.1016/j.marpetgeo.2022.105742>, 2022.
- 466 Wilkinson, M. D., Dumontier, M., Aalbersberg, I. J., Appleton, G., Axton, M., Baak, A., Blomberg, N.,
467 Boiten, J. W., da Silva Santos, L. B., Bourne, P. E., Bouwman, J., Brookes, A. J., Clark, T.,
468 Crosas, M., Dillo, I., Dumon, O., Edmunds, S., Evelo, C. T., Finkers, R., Gonzalez-Beltran, A.,
469 Gray, A. J., Groth, P., Goble, C., Grethe, J. S., Heringa, J., t Hoen, P. A., Hooft, R., Kuhn, T., Kok,
470 R., Kok, J., Lusher, S. J., Martone, M. E., Mons, A., Packer, A. L., Persson, B., Rocca-Serra, P.,
471 Roos, M., van Schaik, R., Sansone, S. A., Schultes, E., Sengstag, T., Slater, T., Strawn, G., Swertz,
472 M. A., Thompson, M., van der Lei, J., van Mulligen, E., Velterop, J., Waagmeester, A.,
473 Wittenburg, P., Wolstencroft, K., Zhao, J., and Mons, B.: The FAIR Guiding Principles for
474 scientific data management and stewardship, *Sci. Data*, 3, 160018,
475 <https://doi.org/10.1038/sdata.2016.18>, 2016.
- 476 Xiang, L., Schoepfer, S. D., Zhang, H., Cao, C., and Shen, S.: Evolution of primary producers and



477 productivity across the Ediacaran-Cambrian transition, *Precambrian Res.*, 313, 68-77,
478 <https://doi.org/10.1016/j.precamres.2018.05.023>, 2018.

479 Zhang, Q., Bendif, E. M., Zhou, Y., Nevado, B., Shafiee, R., and Rickaby, R. E. M.: Declining metal
480 availability in the Mesozoic seawater reflected in phytoplankton succession, *Nat. Geosci.*, 15,
481 932-941, <https://doi.org/10.1038/s41561-022-01053-7>, 2022.

482 Zhao, K., Zhu, G., Li, T., Chen, Z., and Li, S.: Fluctuations of continental chemical weathering control
483 primary productivity and redox conditions during the Earliest Cambrian, *Geol. J.*, 58, 3659-3672,
484 <https://doi.org/3659-3672>, [10.1002/gj.4778](https://doi.org/10.1002/gj.4778), 2023.